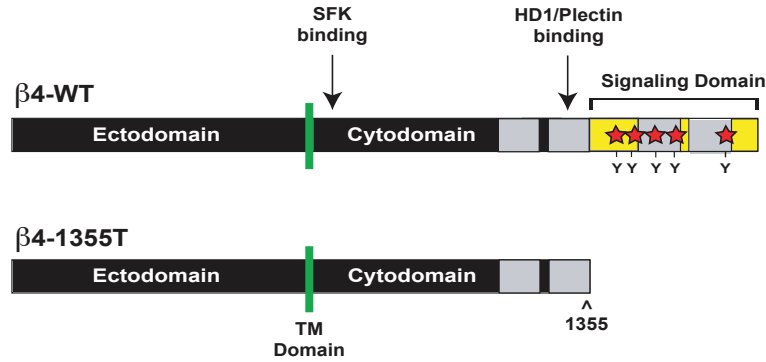
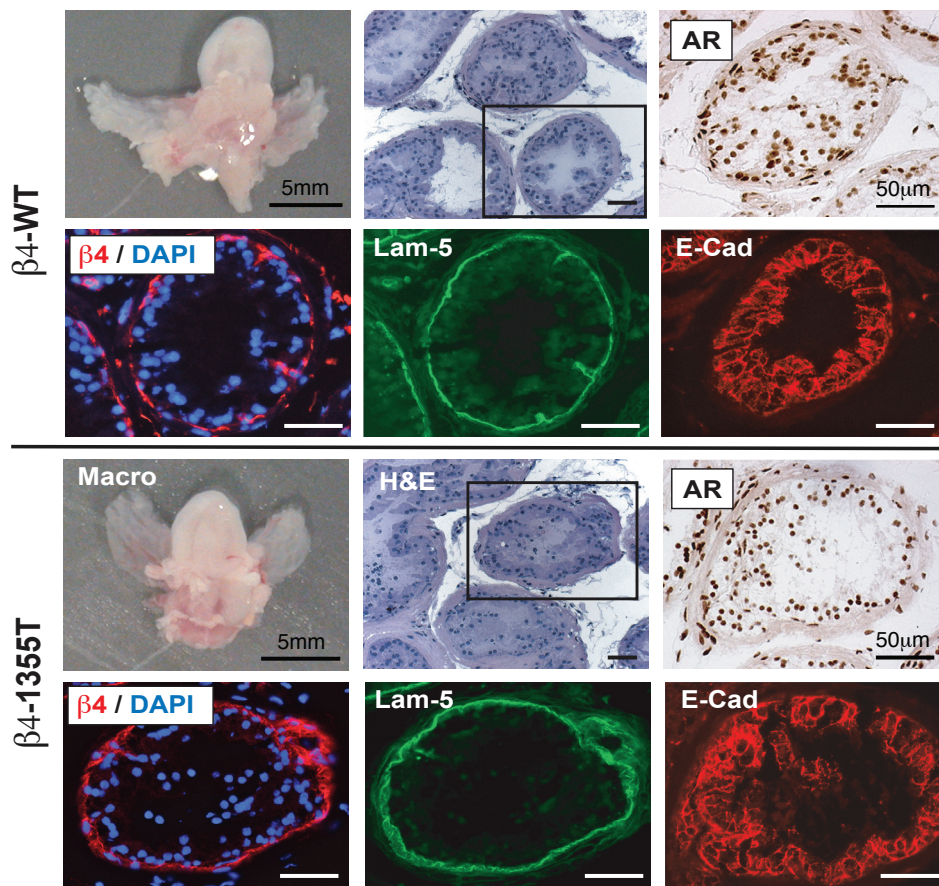
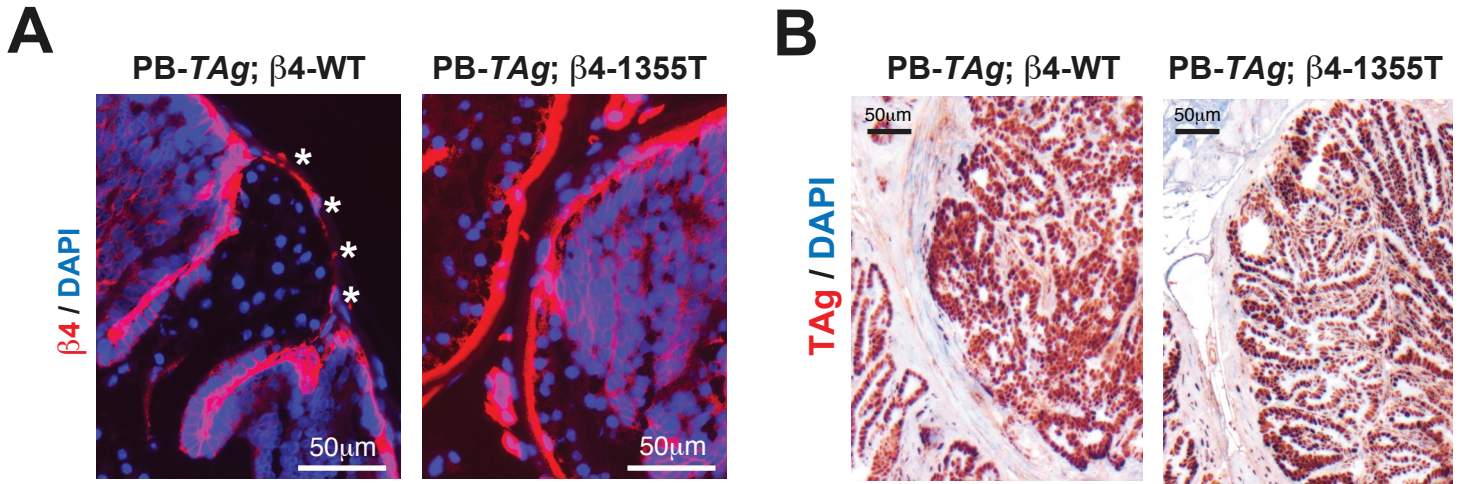


Supplementary Figure 1

Expression of $\beta 4$ in human prostate cancer. **(A)** The graph shows the relative levels of $\beta 4$ mRNA in the indicated normal and tumor samples from the Holzbeierlein DNA microarray dataset. Data are expressed in arbitrary units. **(B)** Equal amounts of total RNA from DU145 cells and the indicated human surgical samples, including normal prostate and four primary tumors, were extracted and subjected to RT-PCR with primers design to amplify the indicated mRNAs. As a negative control (Control), the DU145 RNA was processed for RT-PCR omitting reverse transcriptase. **(C)** A sample of an RT-PCR positive prostate cancer was cut in half and either fixed with formalin and embedded with paraffin or frozen. Whereas sections of the fixed sample close to the separation surface were stained with H&E or subjected to immunohistochemistry with anti-ELF1, sections from the frozen sample were subjected to immunofluorescent staining with anti-ELF1. **(D)** Equal amounts of total lysates of LNCaP cells transduced with empty vector or vector encoding recombinant human $\beta 4$ were subjected to immunoblotting with the anti- $\beta 4$ Mab 439-9B or anti- β -actin. **(E)** Adjacent prostate adenocarcinoma sections were stained with the indicated anti- $\beta 4$ monoclonal antibodies and counterstained with Hematoxylin.

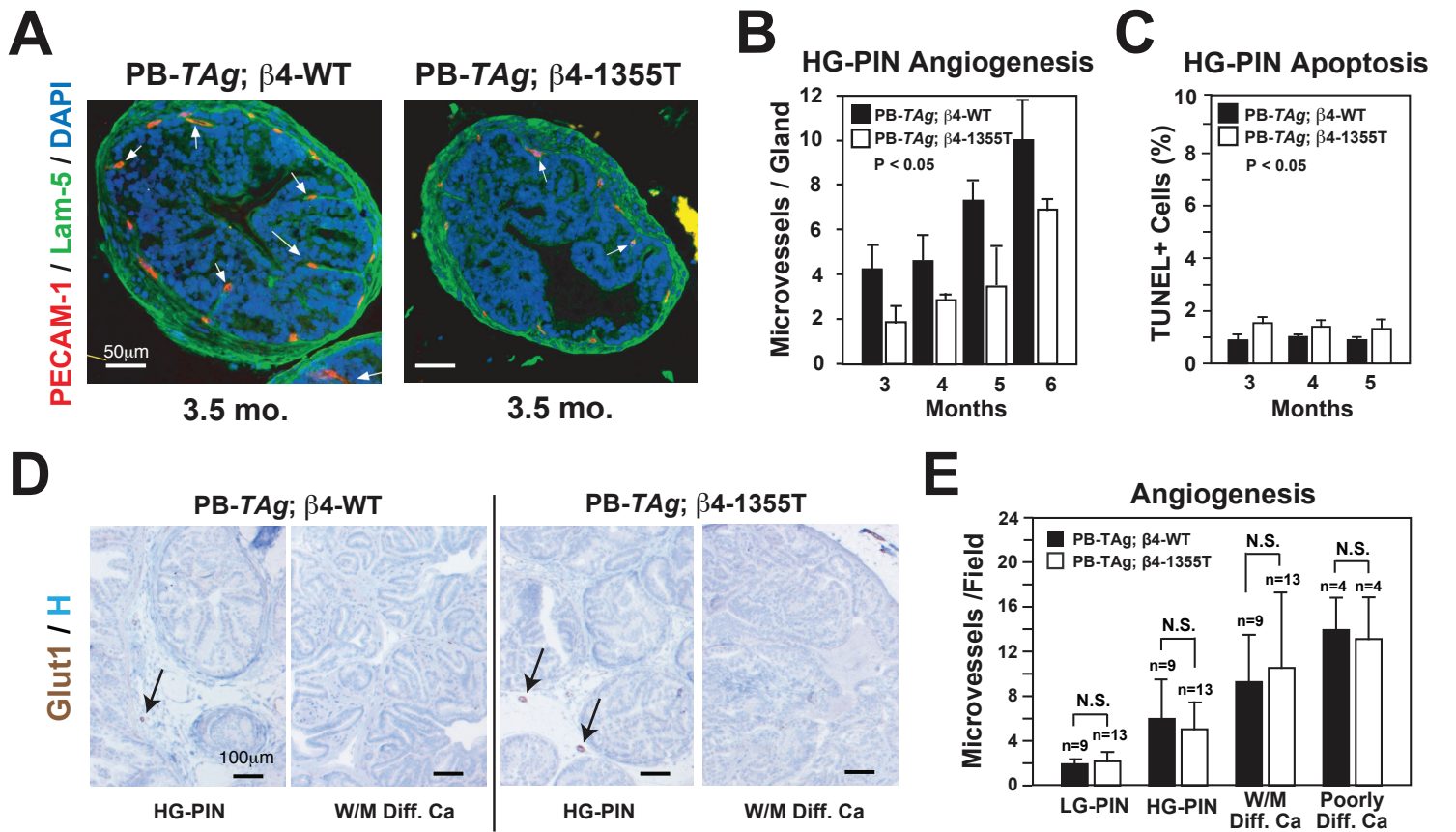
A**B****Supplementary Figure 2**

Deletion of the $\beta 4$ signaling domain does not cause obvious defects in prostate development. (A) The major functional domains of $\beta 4$ and the segment deleted by the 1355T mutation are indicated. Grey rectangles represent FN type III repeats. Stars indicate the major tyrosine phosphorylation sites. Binding to HD-1/Plectin is sufficient for assembly of hemidesmosomes in vivo. (B) Urogenital organs were dissected en bloc from 3 month-old $\beta 4$ -wt and $\beta 4$ -1355T mice and photographed (Macro). Paraffin-embedded sections were stained with H&E. Frozen sections were stained with antiandrogen receptor (AR), anti- $\beta 4$ and DAPI ($\beta 4$ /DAPI), anti-laminin-5 (Lam-5), or anti E-Cadherin (E-Cad).



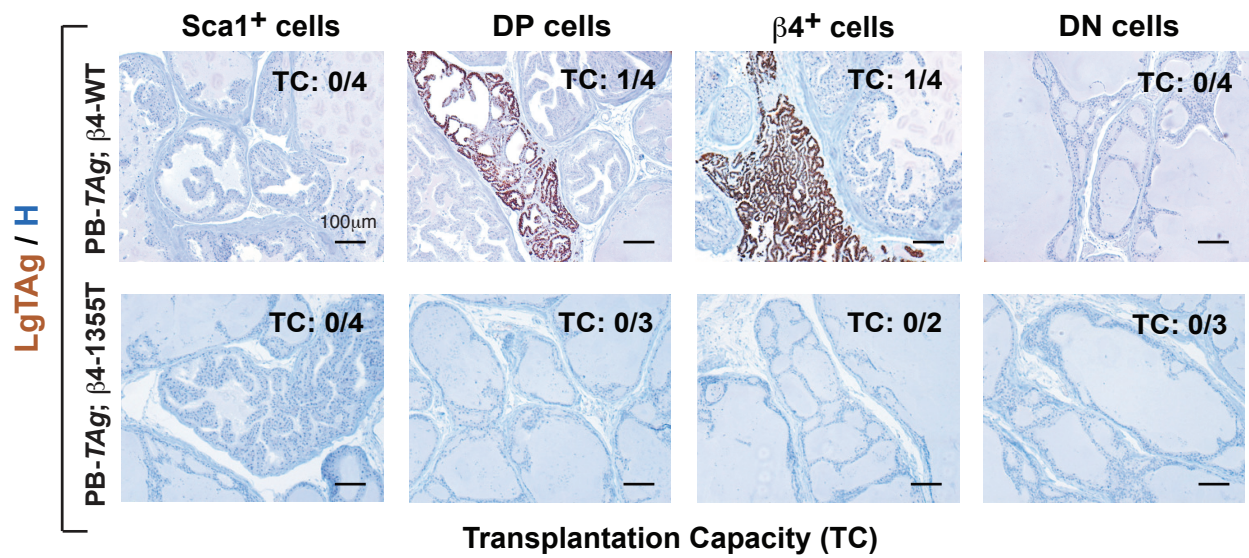
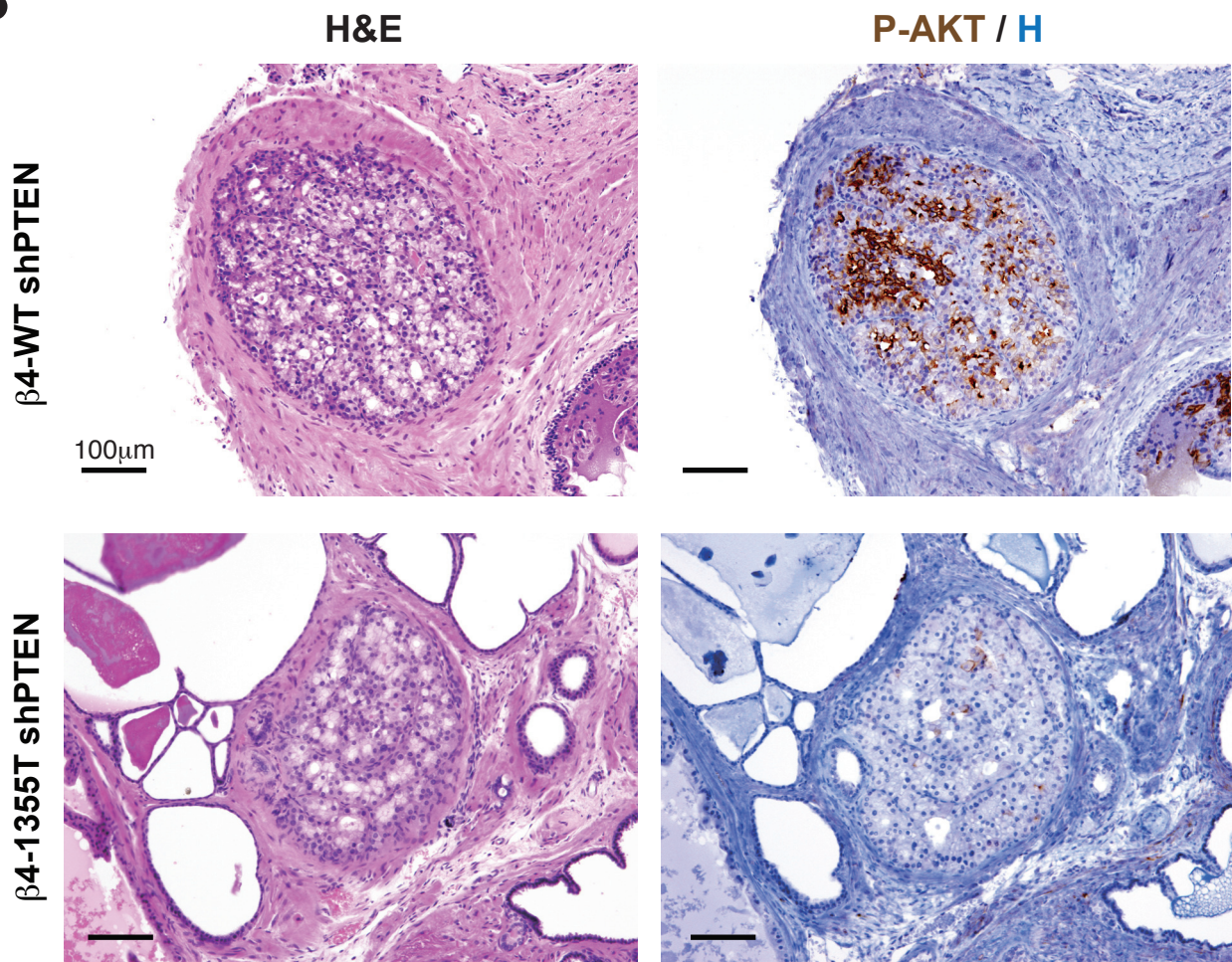
Supplementary Figure 3

Deletion of the b4 signaling domain does not impair expression and basal localization of α 6 β 4 or expression of the T antigen in PB-*TAg* mice. **(A)** High-grade PIN lesions from mice of the indicated genotypes were stained with anti- β 4 and counterstained with DAPI. **(B)** High-grade PIN lesions from mice of the indicated genotypes were stained with antibodies to the AR and counterstained with DAPI.

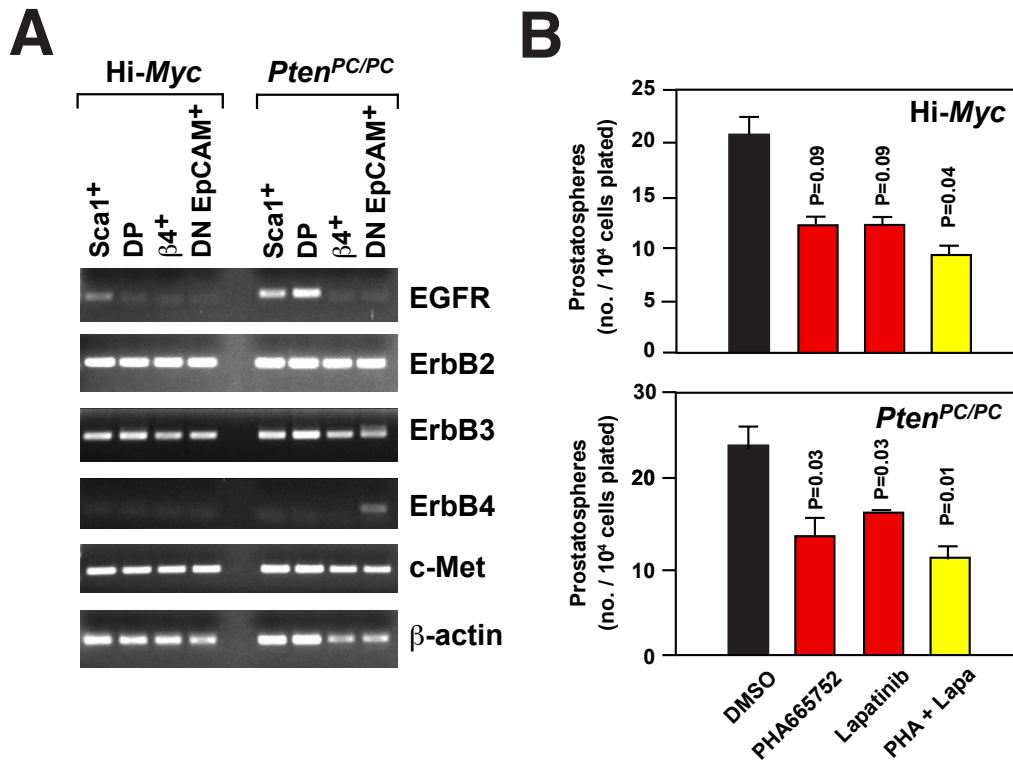


Supplementary Figure 4

Deletion of the $\beta 4$ signaling domain does not induce tumor hypoxia or apoptosis as a consequence of reduced neovascularization. **(A)** High-grade PIN lesions from 3.5 months old PB-TAg/ $\beta 4$ wt and PB-TAg/ $\beta 4$ -1355T mice were subjected to double staining with anti-PECAM-1 and anti-Laminin-5 followed by counterstaining with DAPI. White arrows point to intraductal microvessels and yellow arrows to interductal vessels. **(B)** The graph shows the mean (\pm SD) number of intraductal microvessels in high-grade PIN lesions from mice of the indicated genotypes at the indicated times (n=3 per group). **(C)** High-grade PIN lesions from PB-TAg/ $\beta 4$ -WT and PB-TAg/ $\beta 4$ -1355T mice were subjected to TUNEL staining. The graph plots the mean (\pm SD) percentage of apoptotic cells detected at 3, 4, and 5 months (n=3 per group). **(D)** sections of high-grade PIN lesions and carcinomas from mice of the indicated genotypes were stained with antibodies to the hypoxia-induced Glut1 transporter followed by counterstaining with Hematoxylin. Arrows point to isolated Glut1-positive stromal cells. **(E)** The graph shows the mean (\pm SD) number of microvessels per microscopic field in low-grade (LG) PIN lesions, high-grade (HG) PIN lesions, well and moderately (W/M) differentiated adenocarcinomas, and poorly differentiated carcinomas from mice of the indicated genotypes.

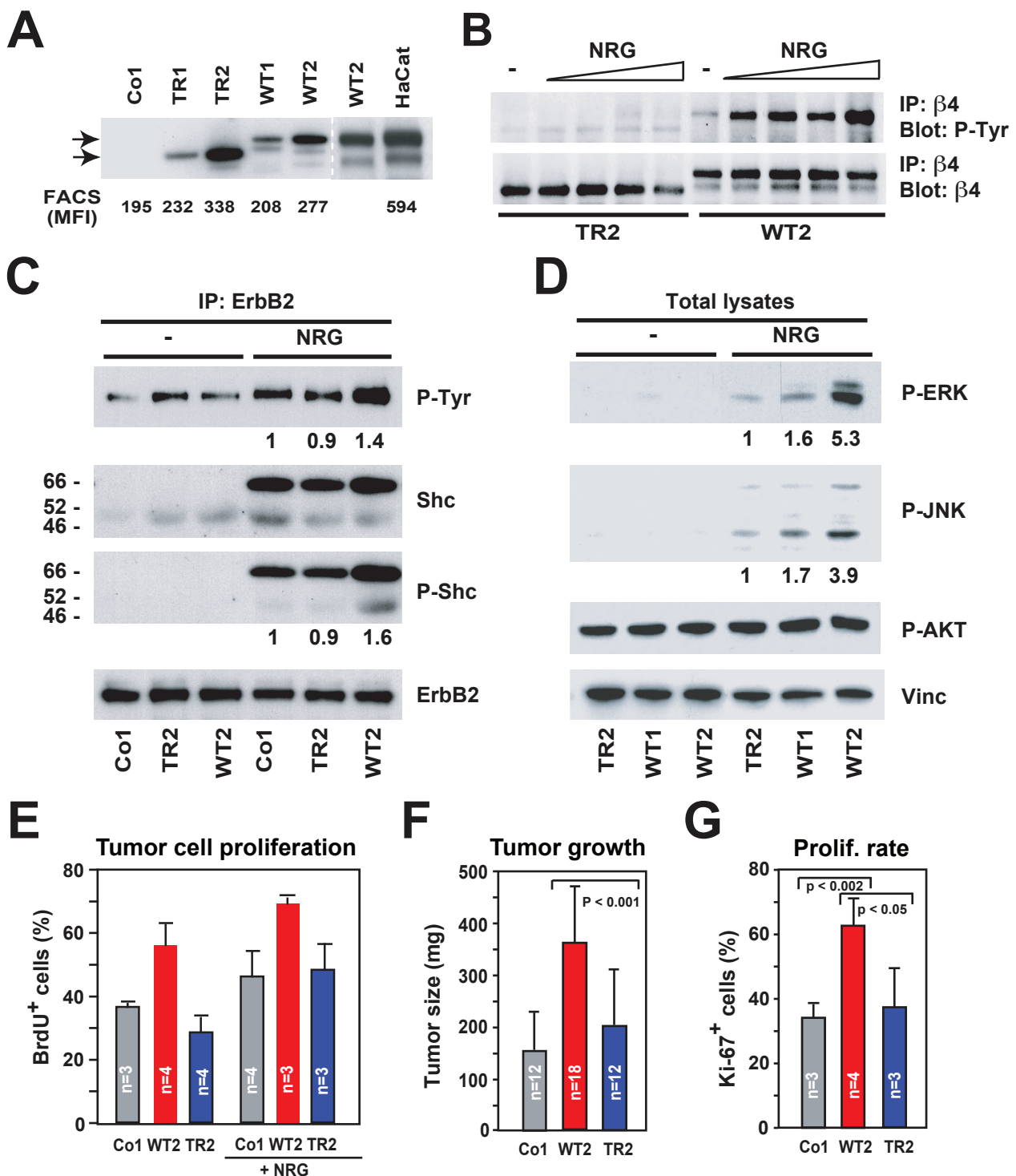
A**B****Supplementary Figure 5**

Deletion of the β 4 signaling domain impairs prostate cancer transplantation efficiency. **(A)** Tumors from 4.5 month-old PB-TAG; β 4-WT and 6.5 month old PB-TAG; β 4-1355T mice were dissociated and sorted into four subpopulations after gating for Lin⁻ cells. To exclude mesenchymal components from the DN cells, EpCAM⁻ cells were excluded. Cells were injected orthotopically in immunocompromised mice at 50×10^3 per mouse. The presence of secondary tumors was assessed 60 days later by using immunohistochemistry with antibodies to the SV40 LT Ag. Samples were counterstained with Hematoxylin (H). The number of positive and total number of cases is shown for each experimental group. **(B)** Prostate epithelial cells from mice of the indicated genotypes were subjected to Pten silencing in vitro and injected under the renal capsule of NOD-SCID-IL2R $\gamma^{-/-}$ mice together with USGM cells. Sections including PIN lesions of comparable size were stained as indicated.



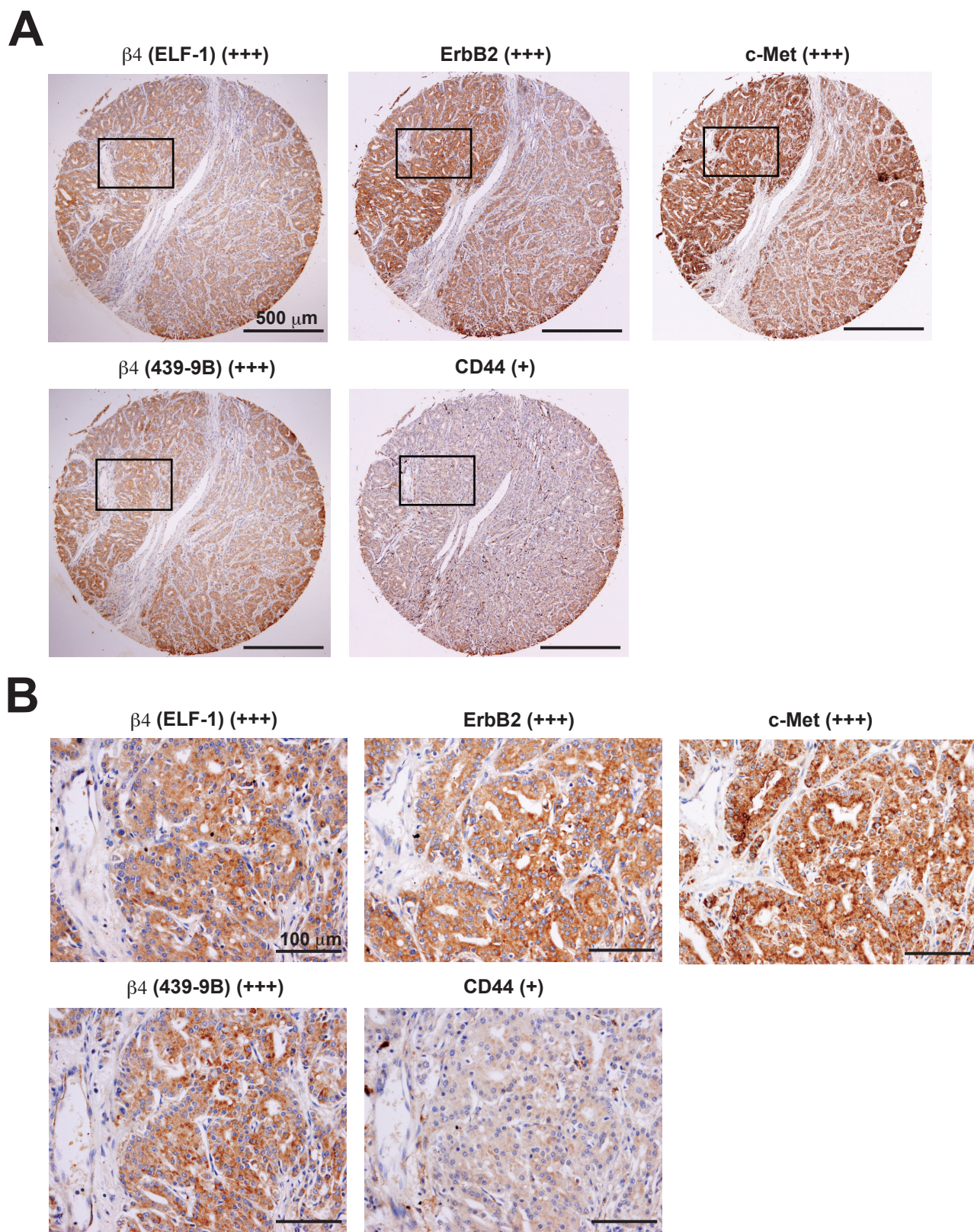
Supplementary Figure 6

ErbB2 and c-Met sustain the self-renewal capability of prostate tumor progenitor cells from Hi-Myc and Pten^{PC/PC} mice. **(A)** Dissociated total tumor cells and the indicated subpopulations from prostates of Hi-Myc and Pten^{PC/PC} mice were subjected to semi-quantitative RT-PCR to assess expression of the indicated mRNAs. **(B)** DP tumor cells from Hi-Myc and Pten^{PC/PC} mice were assayed for sphere-forming capability in the presence of 100 nM PHA665752, 100 nM Lapatinib, or both. Graph shows the mean (+ SEM) of the number of spheres per 10,000 cells after 12 days of culture.



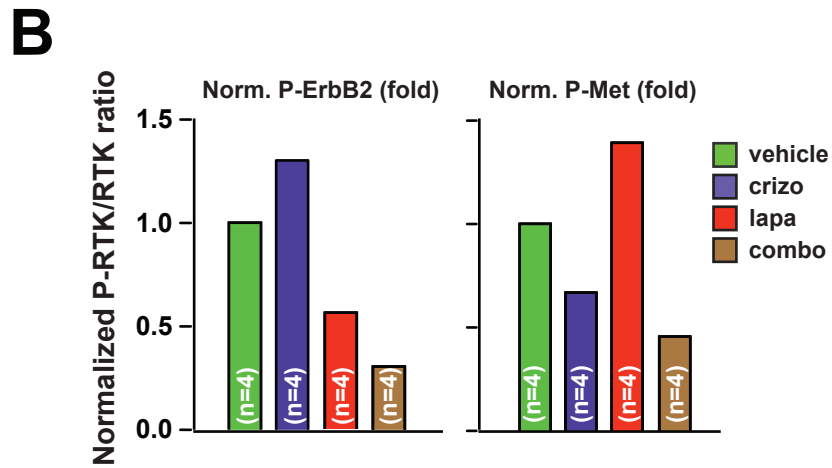
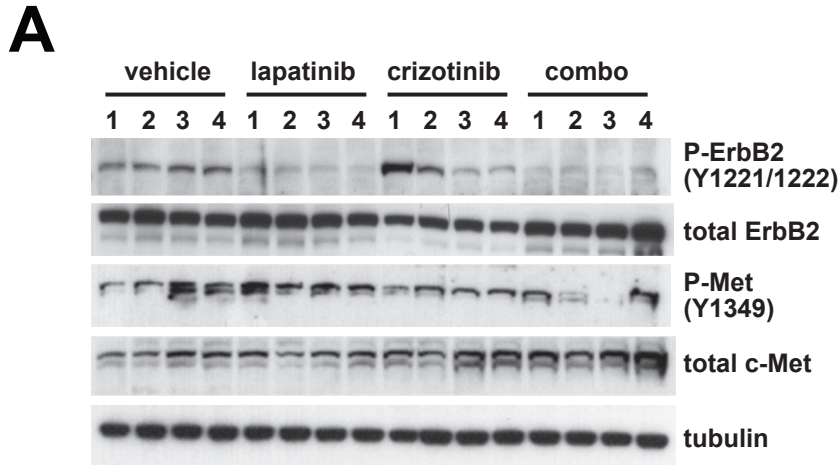
Supplementary Figure 7

Introduction of wild type, but not signaling-defective, $\beta 4$ amplifies ErbB2 signaling, cell proliferation, and tumorigenicity in the AR-dependent LNCaP prostate cancer cells. **(A)** Control LNCaP (Co-1), LNCaP cells stably transfected with $\beta 4$ -WT (WT-1 and -2) or $\beta 4$ -1355T (TR-1 and -2), and HaCat keratinocytes were subjected to immunoblotting and FACS analysis with anti- $\beta 4$. Mean fluorescent intensity (MFI) values are indicated below. **(B)** TR2 and WT2 cells were deprived of growth factors for 24 hours and either left untreated or stimulated with 40, 100, 200, and 400 ng/ml NRG for 10 minutes. Anti- $\beta 4$ immunoprecipitates were blotted with either anti-Phospho-Tyr or anti- $\beta 4$. **(C)** After growth factor starvation, the indicated cells were left untreated or stimulated with 40 ng/ml NRG for 10 minutes. Anti-ErbB2 immunoprecipitates were blotted with the indicated antibodies. The relative level of intensity of relevant bands was estimated by densitometry and normalized to ErbB2 levels. **(D)** The indicated cells were deprived of growth factors, detached, and plated on laminin-5 for 60 minutes in the absence or presence of 100 ng/ml NRG. Total lysates were subjected to blotting with the indicated antibodies. The relative intensity of relevant bands in the boxed areas was normalized to vinculin. **(E)** The indicated cells were cultured in medium containing 10% FBS with or without 50 ng/ml NRG. After addition of BrdU for 1 hour, the cells were stained with anti-BrdU. The graph shows the mean (\pm SD) percentage of BrdU positive cells. **(F)** The indicated cells were injected subcutaneously at 5×10^6 and allowed to grow for 17 days. The graph shows the mean tumor weight (\pm SD) in the indicated tumor xenografts. **(G)** The graph shows the mean (\pm SD) percentage of Ki-67⁺ tumor cells in the indicated tumor xenograft.



Supplementary Figure 8

Immunohistochemical staining of a prostate adenocarcinoma sample co-expressing $\beta 4$, ErbB2 and c-Met, but not CD44. **(A)** Low magnification pictures of the adjacent sections stained with the indicated antibodies. **(B)** High magnification pictures from the insets in (A).



Supplementary Figure 9

Verification of target inhibition in drug-exposed mice. **(A)** Equal amounts of total proteins from tumor lysates from 4 mice that had been treated for 65 days under the indicated conditions were immunoblotted as indicated. **(B)** Densitometry was used to estimate the ratio of P-ErbB2 to total ErbB2 and P-Met to total c-Met in each sample. The graphs show the results normalized to vehicle control.

Supplementary Table 1
Expression of $\beta 4$ in Human Prostate Cancer Tissue Microarrays

	Intensity of Staining	
	0-1+	2-3+
Cellular compartment: (% cases staining)		
Endothelial cells	0	100
Basal Cells	0	100
Normal Acinar (suprabasal) Cells	95	5
High grade PIN	0	100
Prostatic adenocarcinoma	65	35

Since we noted minimal variability in staining within each cellular compartment, we concentrated on evaluating staining intensity. Intensity was scored from 0 to 3+ with 0 representing no staining, 1+ representing weak but granular cytoplasmic immunoreactivity which usually required examination at 20X magnification. 2+ intensity was moderate staining easily discernible at 10x magnification and 3+ positivity was intense staining at the same magnification.

Supplementary Table 2

Concordance of ELF-1 and 439-9B staining on TMA-39

	β 4(ELF-1)	β 4(439-9B)
1	+++	+++
2	+++	+++
3	++	++
4	++	++
5	++	+
6	++	++
7	++	++
8	++	++
9	++	+
10	+	+
11	+	++
12	++	+
13	+	++
14	+	+
15	+	+
16	-	-
17	+	+
18	++	++
19	++	++
20	+	+
21	+	+
22	+	+
23	+	+
24	++	++
25	++	++
26	++	++
27	++	++
28	-	-
29	-	-
30	+	+
31	++	+++
32	++	++
33	++	++
34	+	+
35	++	++
36	-	-
37	++	++
38	+	+
39	+	++

Supplementary Table 3

Clinical and pathological annotation of TMA-39

	Sex	Age	Pathological diagnosis	Gleson score	TNM	Stage	PSA (ng/ml)
1	M	64	Adenocarcinoma	7	T2cN0M0	ii	30
2	M	71	Adenocarcinoma	9	T3bN0M0	III	60.4
3	M	64	Adenocarcinoma	10	T3aN0M0	III	7.4
4	M	59	Adenocarcinoma	9	T3bN0M0	III	9.8
5	M	65	Adenocarcinoma	8	T4N0M0	IV	34.9
6	M	73	Adenocarcinoma	7	T2cN0M0	II	48.1
7	M	69	Adenocarcinoma	7	T2cN0M1	II	10.6
8	M	62	Adenocarcinoma	7	T2cN0M1	II	37.3
9	M	66	Adenocarcinoma	9	T3bN0M0	III	1.2
10	M	60	Adenocarcinoma	9	T3bN0M0	III	40
11	M	70	Adenocarcinoma	7	T4N0M0	IV	7
12	M	65	Adenocarcinoma	9	T3bN0M1	III	17.5
13	M	67	Adenocarcinoma	9	T3bN1M0	IV	13.1
14	M	69	Adenocarcinoma	7	T3bN0M0	III	1.1
15	M	69	Adenocarcinoma	7	T3aN0M1	III	17.6
16	M	70	Adenocarcinoma	7	T3aN0M1	III	9
17	M	58	Adenocarcinoma	9	T3bN0M0	III	5.8
18	M	71	Adenocarcinoma	7	T2cN0M0	II	31.4
19	M	70	Adenocarcinoma	7	T3bN0M0	III	14.4
20	M	59	Adenocarcinoma	6	T2bN0M0	II	18.3
21	M	63	Adenocarcinoma	9	T3bN0M0	III	16.6
22	M	72	Adenocarcinoma	9	T3bN0M0	III	-
23	M	66	Adenocarcinoma	8	T3bN0M0	III	10.8
24	M	70	Adenocarcinoma	7	T2cN0M1	II	-
25	M	68	Adenocarcinoma	8	T3bN0M0	III	26.9
26	M	63	Adenocarcinoma	10	T3bN0M1	III	-
27	M	57	Adenocarcinoma	7	T3bN0M0	III	25
28	M	72	Adenocarcinoma	8	T2cN0M0	III	16.8
29	M	70	Adenocarcinoma	8	T3bN0M0	III	0.5
30	M	75	Adenocarcinoma	9	T3bN0M0	III	98
31	M	62	Adenocarcinoma	9	T3bN0M0	III	-
32	M	63	Adenocarcinoma	9	T3bN0M0	III	91
33	M	53	Adenocarcinoma	9	T3bN0M0	III	161
34	M	63	Adenocarcinoma	8	T3bN0M0	III	13
35	M	44	Adenocarcinoma	7	T3bN0M1	III	-
36	M	65	Metastasis to the abdominal wall			IV	-
37	M	61	Bone metastasis			IV	-
38	M	69	Bone metastasis			IV	-
39	M	59	Bone metastasis			IV	-

Supplementary Table 4

Expression of β 4, HER2, c-Met, and CD44 in prostate cancer TMA-35

	β 4(ELF-1)	β 4(439-9B)	ErbB2	c-Met	CD44
1	+++	+++	+++	+++	+
2	+	+	+	++	+
3	++	++	+++	+++	++
4	+	+	++	++	-
5	+++	++	+++	+++	++
6	++	++	++	+++	++
7	++	++	++	++	++
8	++	++	++	++	+
9	++	++	++	++	-
10	++	++	++	+	++
11	-	-	+	+	+
12	+	+	+	-	-
13	++	++	++	+++	++
14	++	++	++	++	++
15	+	+	++	++	+
16	+++	++	+++	+++	++
17	++	++	++	++	++
18	+	+	+	+	+
19	++	+	++	++	+
20	++	++	++	++	++
21	++	++	++	++	+
22	+++	++	+++	+++	++
23	++	++	++	++	++
24	++	+	++	+	+
25	++	++	++	++	++
26	++	++	++	+++	-
27	+	+	+	++	++
28	++	++	++	++	+
29	++	+	++	++	+
30	+	+	+	++	-
31	+++	++	++	+++	+
32	++	++	++	+++	++
33	++	++	++	++	++
34	++	++	++	+++	++
35	++	++	++	+++	++

Supplementary Table S5

Clinical and pathological annotation of TMA-35

	Sex	Age	Pathological diagnosis	Gleson score	TNM	Stage	PSA (ng/ml)
1	M	70	Adenocarcinoma	6	T2N0M0	ii	-
2	M	70	Adenocarcinoma	5	T2aN0M0	II	-
3	M	60	Adenocarcinoma	9	T4N1M1c	IV	-
4	M	61	Adenocarcinoma	5	T2N0M0	ii	-
5	M	66	Adenocarcinoma	5	T3N1M1	IV	-
6	M	75	Adenocarcinoma	9	T3N0M1b	IV	-
7	M	76	Adenocarcinoma	4	T2aN0M0	II	-
8	M	64	Adenocarcinoma	5	T3N0M1	IV	-
9	M	69	Adenocarcinoma	7	T2N0M0	II	-
10	M	64	Adenocarcinoma	7	T3N0M1b	IV	-
11	M	69	Adenocarcinoma	6	T2N0M0	II	-
12	M	70	Adenocarcinoma	9	T2N0M0	II	-
13	M	65	Adenocarcinoma	7	T2N0M0	II	-
14	M	73	Adenocarcinoma	4	T2N0M0	II	-
15	M	55	Adenocarcinoma	3	T2N0M0	II	-
16	M	72	Adenocarcinoma	7	T2N0M0	II	-
17	M	62	Adenocarcinoma	6	T3N1M1b	IV	-
18	M	73	Adenocarcinoma	7	T3N0M1b	IV	-
19	M	70	Adenocarcinoma	6	T2N0M0	II	-
20	M	80	Adenocarcinoma	8	T4N1M1c	IV	-
21	M	69	Adenocarcinoma	6	T3N0M0	III	-
22	M	58	Adenocarcinoma	6	T2N0M0	II	-
23	M	73	Adenocarcinoma	8	T3N1M1c	IV	-
24	M	70	Adenocarcinoma	7	T2bN0M0	II	-
25	M	65	Adenocarcinoma	7	T2N1M1	IV	-
26	M	64	Adenocarcinoma	8	T2N0M0	II	-
27	M	60	Adenocarcinoma	8	T3N1M1b	IV	-
28	M	70	Adenocarcinoma	6	T3N0M0	III	-
29	M	73	Adenocarcinoma	10	T4N1M1c	IV	-
30	M	76	Adenocarcinoma	9	T3N1M1b	IV	-
31	M	73	Adenocarcinoma	6	T3N1M1b	IV	-
32	M	55	Adenocarcinoma	7	T2N0M0	II	-
33	M	63	Adenocarcinoma	7	T2N1M1b	IV	-
34	M	60	Adenocarcinoma	8	T2N0M0	II	-
35	M	82	Adenocarcinoma	8	T2N0M0	II	-